

Testing the validity of the phenomenological gravitational waveform models for nonspinning binary black hole searches at low masses

Hee-Suk Cho

E-mail: chohs1439@pusan.ac.kr

Korea Institute of Science and Technology Information, Daejeon 305-806, Korea

Abstract. The phenomenological gravitational waveform models, i.e. the PhenomA, the PhenomB and the PhenomC, generate full inspiral-merger-ringdown waveforms of coalescing binary black holes (BBHs). These models are defined in the Fourier domain and thus can be used for fast matched filtering in the gravitational wave search. The PhenomA has been developed for nonspinning BBH waveforms, while the PhenomB and the PhenomC can model the nonprecessing BBH waveforms. In this work, we study the validity of the phenomenological models for nonspinning BBH searches at low masses, $m_{1,2} \geq 4M_{\odot}$ and $m_1 + m_2 \equiv M \leq 30M_{\odot}$, with Advanced LIGO sensitivity. As our complete signal waveform model, we adopt the EOBNRv2 that is a time domain inspiral-merger-ringdown waveform model. To investigate the search efficiency of the phenomenological templates, we calculate fitting factors by exploring overlap surfaces. We find that only the PhenomC is valid to obtain the fitting factors better than 0.97 in the mass range of $M < 15M_{\odot}$. Above $15M_{\odot}$, the PhenomA is most efficient in symmetric mass region, the PhenomB is most efficient in highly asymmetric mass region, and the PhenomC is most efficient in the intermediate region. Especially, we propose an effective phenomenological template family that can be constructed by employing the phenomenological models in four subregions individually. We find that fitting factors of the effective templates are better than 0.97 in our entire mass region and mostly greater than 0.99.

Keywords: gravitational waves, compact binary coalescence, phenomenological waveforms

PACS numbers: 04.30.-w, 04.30.Db, 04.30.Tv

1. Introduction

Coalescing binary black holes (BBHs) are among the most promising sources of gravitational wave (GW) transients for ground-based detectors, such as LIGO [1] and Virgo [2]. GW signals emitted from BBHs are conventionally divided into three phases: inspiral, merger and ringdown (IMR). Inspiral waveforms can be accurately obtained by using post-Newtonian (PN) approximations. When the system reaches the ultra-relativistic regime, however, merger-ringdown waveforms should be calculated from

numerical relativity (NR) simulations. A full IMR waveform can be constructed by combining a PN inspiral waveform and a NR merger-ringdown waveform. However, obtaining merger-ringdown waveforms from NR simulations is computationally very expensive. Thus, inspiral waveforms have mainly been used for low mass binaries below $\sim 30M_{\odot}$ in ground-based GW data analyses [3]. It has been anticipated that the inspiral waveforms would yield accurate analysis results for low mass binaries because in those systems the inspiral phase is likely to have most of the signal power in detection frequency band of ground-based detectors.

However, several authors have pointed out that the absence of the merger-ringdown phase can decrease the search efficiency, thus induce a non-negligible loss in the detection rate, even for low mass systems. A detection rate tends to decrease with increasing total mass (M), and that becomes smaller than 90% when M exceeds some critical value M_{crit} . Buonanno *et al* [4] and Brown *et al* [5] showed that $M_{\text{crit}} \sim 12M_{\odot}$ for various PN inspiral templates with EOBNR signals. Ajith [6] found that $M_{\text{crit}} \sim 15M_{\odot}$ for 3.5PN TaylorT1 inspiral templates with PhenomA signals. Recently, Cho [7] carried out a careful analysis using inspiral templates and PhenomA signals, and also obtained $M_{\text{crit}} \sim 15M_{\odot}$, in which the inspiral waveforms were constructed by taking the inspiral parts into account from the PhenomA waveforms to avoid the systematic effect that arises when the model for signals is difference from the model for templates.

Efforts to establish the analytic IMR waveform models have been made over the past years. Those works have been carried out by constructing phenomenological family of waveforms in the Fourier domain by using PN-NR hybrid waveforms. The first phenomenological family (PhenomA), which can model the IMR waveforms of nonspinning BBHs, has been proposed by Ajith *et al* [8, 9, 6]. The second family (PhenomB) has been developed by Ajith *et al* [10] by extending the PhenomA to the case of nonprecessing BBHs. The third family (PhenomC) has been made by Sanataria *et al* [11] for nonprecessing BBHs. The recent phenomenological family (PhenomP) allows us to have IMR waveforms of precessing BBHs [12]. On the other hand, a time domain IMR waveform model has also been developed using an effective-one-body (EOB) approach. The accuracy of EOB waveforms has been improved by calibrating them to NR waveforms. The stability of the nonspinning EOB model has been investigated by Pan *et al* [13]. They showed that those waveforms of any length are sufficiently accurate for data analysis with advanced GW detectors. Recently, in addition, that has been robustly confirmed by Szilágyi *et al* [14] by using a long NR simulation of a compact binary whose gravitational waveform is long enough to cover the entire frequency band of advanced GW detectors. They also found that existing phenomenological IMR waveforms display much greater disagreement with the NR simulation.

In this work, we adopt as our complete signal waveform model the EOBNRv2 described in [15]. We take into account all the spherical harmonics modes of the EOBNRv2 waveforms available in the LSC Algorithm Library (LAL) [16], those are the leading (2, 2) mode and the four sub-leading modes (2, 1), (3, 3), (4, 4) and (5

,5). We test the validity of the phenomenological template models in GW searches for nonspinning BBHs at low masses with Advanced LIGO sensitivity. The result is summarised in section 3.2. Especially, we propose an effective template family that always has the fitting factors better than 0.97 in low mass region. Because the phenomenological fitting coefficients of the PhenomB are defined differently from those of the PhenomA, the PhenomB waveform with masses (m_1, m_2) and a zero spin are different from the PhenomA waveform with the same masses. While, the PhenomP waveform with masses (m_1, m_2) and a zero spin is the same as the PhenomC waveform with the same masses and a zero spin because the PhenomP is derived from the PhenomC by adding an effective precession spin. Therefore, we only consider the PhenomA, the PhenomB and the PhenomC models for our nonspinning BBHs. When using the PhenomB and the PhenomC as our templates, we will neglect the spin effect by choosing zero spins in the wave functions. Note that we follow the naming convention defined in the LAL for the phenomenological models in this work.

2. Phenomenological waveforms

Obtaining phenomenological models involves finding fitting parameters of the analytic waveform family using PN-NR hybrid waveforms. The phenomenological waveform families are defined in the Fourier domain as the form,

$$\tilde{h}_{\text{phen}}(f) = A_{\text{eff}}(f) e^{\Psi_{\text{eff}}(f)}, \quad (1)$$

where the effective amplitude $A_{\text{eff}}(f)$ and the effective phase $\Psi_{\text{eff}}(f)$, and those are modeled separately. The model waveforms are parameterised by their physical parameters such as total mass M , symmetric mass ratio $\eta = m_1 m_2 / M^2$ and spin parameter χ . In this section, we only provide the functional forms of the phenomenological models. More details can be found in [8, 9, 6], [10] and [11] for the PhenomA, the PhenomB and the PhenomC, respectively.

2.1. PhenomA

Amplitude spectrum of a PhenomA waveform is divided by two phenomenological frequencies, f_{merg} and f_{ring} , and terminates at the cutoff frequency f_{cut} :

$$A_{\text{eff}} = A f_{\text{merg}}^{-7/6} \begin{cases} (f/f_{\text{merg}})^{-7/6} & \text{if } f < f_{\text{merg}} \\ (f/f_{\text{merg}})^{-2/3} & \text{if } f_{\text{merg}} \leq f < f_{\text{ring}} \\ w \mathcal{L}(f, f_{\text{ring}}, \bar{\sigma}) & \text{if } f_{\text{ring}} \leq f \leq f_{\text{cut}}, \end{cases} \quad (2)$$

where A is the wave amplitude factor whose value depends on the binary masses and five extrinsic parameters determined by the sky location and the binary orientation. $\mathcal{L}(f, f_{\text{ring}}, \bar{\sigma}) \equiv \left(\frac{1}{2\pi}\right) \frac{\bar{\sigma}}{(f-f_{\text{ring}})^2 + \bar{\sigma}^2/4}$ is a Lorentzian function that has a width $\bar{\sigma}$, and that is centered around the frequency f_{ring} . The normalization constant, $w \equiv \frac{\pi\bar{\sigma}}{2} \left(\frac{f_{\text{ring}}}{f_{\text{merg}}}\right)^{-2/3}$, is chosen so as to make $A_{\text{eff}}(f)$ continuous across the transition frequency f_{ring} . The parameter f_{merg} is the frequency at which the power-law changes from $f^{-7/6}$ to $f^{-2/3}$.

The phenomenological parameters f_{merg} , f_{ring} , $\bar{\sigma}$ and f_{cut} are given in terms of M and η . The effective phase is expressed as

$$\Psi_{\text{eff}}(f) = 2\pi f t_c + \phi_c + \frac{1}{\eta} \sum_{k=0}^7 (x_k \eta^2 + y_k \eta + z_k) (\pi M f)^{(k-5)/3}, \quad (3)$$

where t_c and ϕ_c are the coalescence time and the coalescence phase. The coefficients introduced in the phenomenological parameters and the effective phase are tabulated in Table 1 of [6]. The accuracy of the PhenomA templates was examined by using (~ 30) hybrid waveforms finely spaced in the parameter range $m_1/m_2 \equiv q \leq 4$ and $50 \leq M/M_\odot \leq 200$, in which the fitting factors were found to be greater than 0.99 for Initial LIGO, Advanced LIGO and Virgo.

2.2. PhenomB

The PhenomB corresponds to an extended version of the PhenomA to nonprecessing BBHs by incorporating the single spin parameter χ . The effective amplitude is defined by

$$A_{\text{eff}} = A f_1^{-7/6} \begin{cases} (f/f_1)^{-7/6} (1 + \sum_{i=2}^3 \alpha_i v^i) & \text{if } f < f_1 \\ w_m (f/f_1)^{-2/3} (1 + \sum_{i=1}^2 \epsilon_i v^i) & \text{if } f_1 \leq f < f_2 \\ w_r \mathcal{L}(f, f_2, \bar{\sigma}) & \text{if } f_2 \leq f \leq f_{\text{cut}}, \end{cases} \quad (4)$$

where $v \equiv (\pi M f)^{1/3}$, $\alpha_{2,3}$ are given in terms of η and χ , $\epsilon_{1,2}$ are given in terms of χ and the normalization constants w_m and w_r are chosen so as to make $A_{\text{eff}}(f)$ continuous across the transition frequency f_2 and f_1 , respectively. The effective phase is defined by

$$\Psi_{\text{eff}}(f) = 2\pi f t_c + \phi_c + \frac{2}{128\eta v^5} \left(1 + \sum_{k=2}^7 \psi_k v^k \right). \quad (5)$$

The coefficients introduced in this model are tabulated in table 1 of [10]. The PhenomB templates were examined in the parameter range $q \leq 10$, and $M \leq 400M_\odot$, in which the fitting factors were greater than 0.965 for Initial LIGO.

2.3. PhenomC

The PhenomC has also been developed for nonprecessing BBHs. The wave amplitude terminates at $f_{\text{cut}} = 0.15/M$, and that is constructed from two parts as

$$A_{\text{eff}} = A_{\text{PM}}(f) w_{f_0}^- + A_{\text{RD}}(f) w_{f_0}^+, \quad (6)$$

where A_{PM} is the premerger amplitude calculated by a PN inspiral amplitude with the addition of a higher order frequency term:

$$A_{\text{PM}}(f) = A_{\text{PN}}(f) + \gamma_1 f^{5/6}, \quad (7)$$

$$A_{\text{PN}} = C \Omega^{-7/6} \left(1 + \sum_{k=2}^5 \gamma_k \Omega^{k/3} \right), \quad (8)$$

where $\Omega = \pi M f$, and A_{RD} is the ringdown amplitude:

$$A_{\text{RD}} = \delta_i \mathcal{L}'[f, f_{\text{RD}}(a, M), \delta_2 Q(a)] \bar{\sigma} f^{-7/6}, \quad (9)$$

Table 1. Parameter ranges of the phenomenological models valid for nonspinning BBH searches with the given detector sensitivity models.

Model	PhenomA	PhenomB	PhenomC
Mass range [M_{\odot}]	$50 \leq M \leq 200$	$M \leq 400$	$M \leq 350$
Mass ratio range	$q \leq 4$	$q \leq 10$	$q \leq 4$
Detector	Initial LIGO, Virgo, Advanced LIGO	Initial LIGO	Advanced LIGO

where the Lorentzian function is defined by $\mathcal{L}'(f, f_0, \bar{\sigma}) \equiv \bar{\sigma}^2 / [(f - f_0)^2 + \bar{\sigma}/4]$, and Q is the quality factor which depends on the final BH spin a . The two amplitude parts can be combined by tanh-window functions:

$$w_{f_0}^{\pm} = \frac{1}{2} \left[1 \pm \tanh \left(\frac{4(f - f_0)}{d} \right) \right], \quad (10)$$

where $d = 0.005$. The transition frequency f_0 is determined by $f_0 = 0.98f_{\text{RD}}$ where f_{RD} is a ringdown frequency given in terms of M and a . The effective phase is calculated by a complete SPA inspiral phasing ψ_{SPA} , a premerger phasing ψ_{PM} and a ringdown phasing ψ_{RD} as

$$\Psi_{\text{eff}}(f) = \psi_{\text{SPA}} w_{f_1}^- + \psi_{\text{PM}} w_{f_1}^+ w_{f_2}^- + \psi_{\text{RD}} w_{f_2}^+, \quad (11)$$

with $f_1 = 0.1f_{\text{RD}}$, $f_2 = f_{\text{RD}}$ using $d = 0.005$ in the window functions. The premerger and ringdown phasing have the forms

$$\psi_{\text{PM}} = \frac{1}{\eta} (\alpha_1 f^{-5/3} + \alpha_2 f^{-1} + \alpha_3 f^{-1/3} + \alpha_4 + \alpha_5 f^{2/3} + \alpha_6 f), \quad (12)$$

$$\psi_{\text{RD}} = \beta_1 + \beta_2 f, \quad (13)$$

where the α_k coefficients are inspired by the SPA phase, redefined and phenomenologically fitted to agree with the hybrid waveforms, while $\beta_{1,2}$ parameters are not fitted but obtained from the premerger ansatz by taking the value and slope of the phase at the transition point f_{RD} . The coefficients introduced in this model are tabulated in table 2 of [11]. The PhenomC templates were examined in the parameter range $q \leq 4$, and $M \leq 350M_{\odot}$, in which the model fitted the original hybrid waveforms with the fitting factors better than 0.97 for Advanced LIGO.

2.4. Comparison

In table 1, we summarise the parameter ranges, in which the validity of the phenomenological models is confirmed with the detector sensitivity models given in the last row. While the validity of the PhenomA is tested only in high mass region, the PhenomB and the PhenomC are valid in broad mass region. The PhenomB is applicable in wider range of mass ratio $q \leq 10$, while the others are valid only in the range of $q \leq 4$.

Figure 1 shows the Fourier-domain amplitude spectra of the EOBNRv2 and the phenomenological waveforms for a nonspinning binary with masses of $(10, 10)M_{\odot}$. We

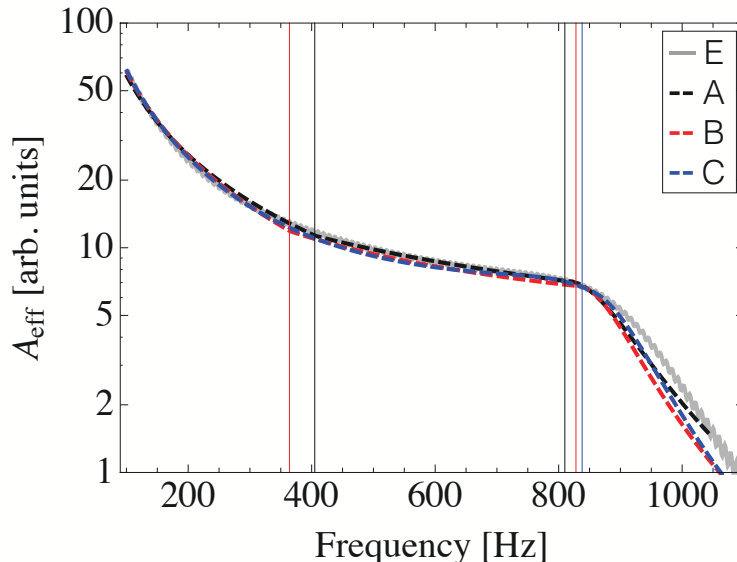


Figure 1. Fourier-domain amplitude spectra of the EOBNRv2 (E), the PhenomA (A), the PhenomB (B) and the PhenomC (C) for a nonspinning BBH with masses $(10,10)M_{\odot}$. The transition frequencies f_{merg} and f_{ring} are denoted by the black (PhenomA) and red (PhenomB) lines, and f_0 (PhenomC) is denoted by the blue line. The small oscillations in the EOBNRv2 spectrum are due to an edge effect in the fast Fourier transform, and this does not affect our analysis.

find that the phenomenological models show similar curves, and those agree well with the amplitude spectrum of the complete EOBNRv2 waveform. While the PhenomA and the PhenomB have two transition frequencies f_{merg} and f_{ring} in the amplitude functions, the PhenomC has one frequency f_0 . Those are also depicted in this figure.

3. Validity of the phenomenological models and the effective template family

3.1. BBH search and fitting factor

The matched filter is the optimal filter for a signal of known shape in stationary Gaussian noise. Because the waveforms emitted from coalescing binaries can be modeled reasonably well, the matched filter can be employed in the search for BBHs. The match between a signal (\tilde{h}_s) and a template (\tilde{h}_t) is expressed by a standard inner product as

$$\langle \tilde{h}_s | \tilde{h}_t \rangle = 4\text{Re} \int_{f_{\text{low}}}^{\infty} \frac{\tilde{h}_s(f) \tilde{h}_t^*(f)}{S_n(f)} df, \quad (14)$$

where $S_n(f)$ is a detector noise power spectral density and f_{low} is a low frequency cutoff of the waveforms that depends on the shape of $S_n(f)$. We use the zero-detuned, high-power noise power spectral density of Advanced LIGO [17], and assume $f_{\text{low}} = 10$ Hz.

When calculating a match, we use the normalized waveform $\hat{h}(f) \equiv \tilde{h}(f) / \langle \tilde{h} | \tilde{h} \rangle^{1/2}$, then the phenomenological models for nonspinning BBHs can be given in terms of

M, η, t_c and ϕ_c for the match calculations. On the other hand, the inverse Fourier transform will compute the match for all possible coalescence times at once and we can also maximize the match over coalescence phases by taking the absolute value of the complex number [18]. The remaining parameters are M and η , and those are main parameters in data analysis for nonspinning binary systems. Note that we use the chirp mass $M_c = M\eta^{3/5}$ instead of M in this work. Therefore, the overlap is defined by maximizing the match over t_c and ϕ_c as

$$P = \max_{t_c, \phi_c} \frac{\langle \tilde{h}_s | \tilde{h}_t \rangle}{\sqrt{\langle \tilde{h}_s | \tilde{h}_s \rangle \langle \tilde{h}_t | \tilde{h}_t \rangle}}. \quad (15)$$

Finally, the fitting factor (FF) is the best-match between two waveforms maximized over all possible parameters [19]. In this work, thus, the FF is obtained by maximizing the overlap over M_c and η as

$$\text{FF} = \max_{M_c, \eta} P(M_c, \eta). \quad (16)$$

For data analysis purposes, the FF is used to evaluate the search efficiency. The gravitational wave searches use a bank of template waveforms constructed in a proper mass range [19, 20, 21, 22]. Typically, a template bank requires that the total mismatch (i.e. 1-FF) between the templates and signals does not exceed 3% [3, 23] including the effect of discreteness of the template spacing. In order to avoid the effect of discreteness, we use sufficiently fine spacings in the $(M_c-\eta)$ plane in this work. The event rate is proportional to the cube of the SNR, and the SNR is calculated by $\rho = \langle \tilde{h}_s | \tilde{h}_s \rangle^{1/2} \text{FF}$. Thus, a FF = 0.97 corresponds to a loss of event rates of $\sim 10\%$.

3.2. FFs of the phenomenological template models

We employ the EOBNRv2 as a complete signal model and the phenomenological models as template models. As describe in Eq. (16), we calculate the FF by exploring a two-dimensional overlap surface finely spaced in the $(M_c-\eta)$ plane. In figure 2, we summarise the FFs of the phenomenological template models for nonspinning BBHs with masses $m_{1,2} \geq 4M_\odot$ and $M \leq 30M_\odot$. The blue, red and black contours correspond to FF = 0.99, 0.98 and 0.97, respectively. This result shows the valid criteria of the Phenomenological template models for nonspinning BBH searches at low mass region. Firstly, although the PhenomA has been tested only in the high mass region $M \geq 50M_\odot$, our result shows that this model is also efficient in the region $M > 12M_\odot$. The PhenomA has been tested in the region $q \leq 4$, and the FFs in our result are also sufficiently high above 0.97 in that region. Secondly, the PhenomB has been examined for Initial LIGO in the range of $M \leq 400M_\odot$, but we find that the FFs can be smaller than 0.97 for Advanced LIGO at the masses below $\sim 15M_\odot$. In addition, the PhenomB has been examined in the range of $q \leq 10$, but our result shows that this model is invalid at symmetric mass region broadly. Finally, the PhenomC has been found to be valid in broad mass region up to $\sim 350M_\odot$ with $q \leq 4$ for Advanced LIGO, and our result also shows that the FFs are overall better than 0.97 in the entire low mass region with $q \leq 4$.

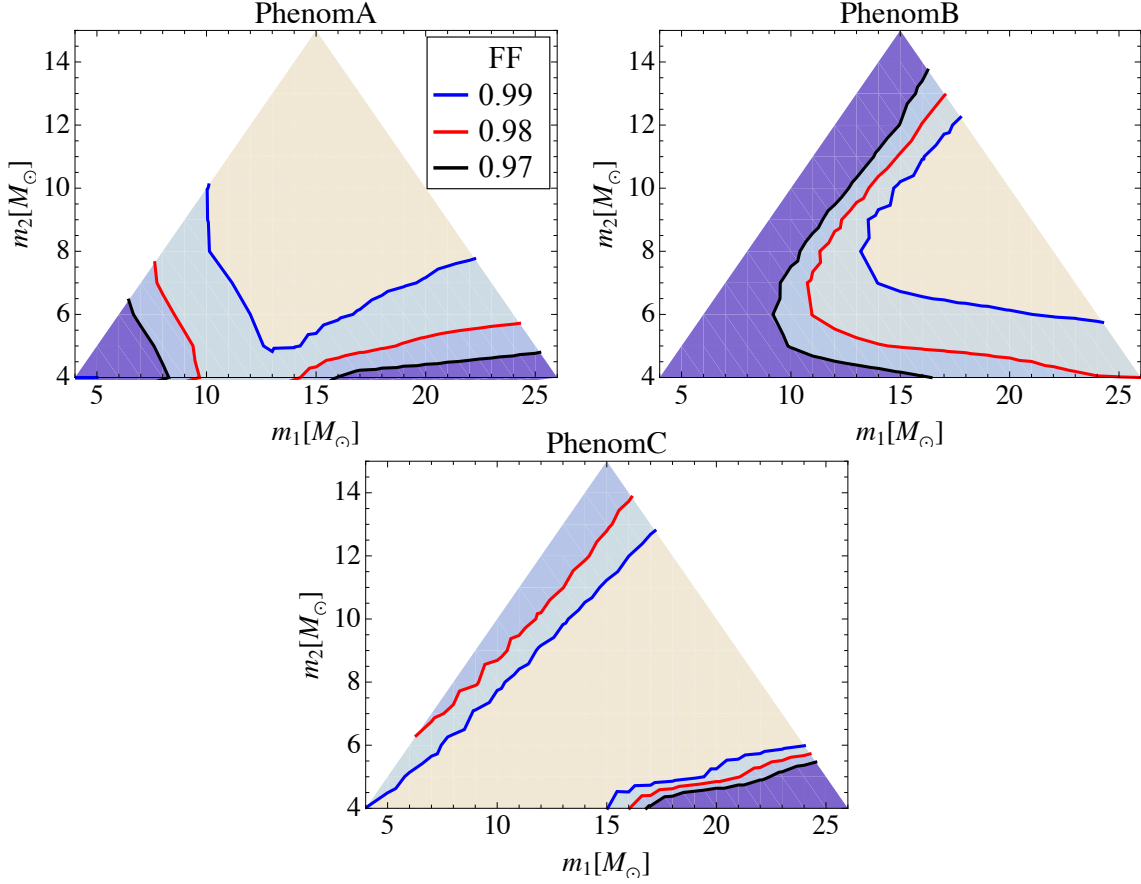


Figure 2. Fitting factors of the phenomenological template models for nonspinning BBHs.

3.3. Constructing the effective phenomenological template family

In figure 2, we can find that the PhenomC is most efficient among the three models for nonspinning BBH searches although that has been developed for nonprecessing BBHs. The FFs of the PhenomC are always better than 0.97 independently of the mass in the region $q \leq 4$. On the other hand, for an arbitrary binary with masses (m_1, m_2) , we can choose one model whose FF is larger than those of the other models. Then, the optimal template family can be obtained by choosing the models individually for all binary masses in our mass region. The FF of the optimal template can be defined by

$$\mathcal{FF}(m_1, m_2) = \text{Max}[A(m_1, m_2), B(m_1, m_2), C(m_1, m_2)], \quad (17)$$

where $\alpha(m_1, m_2)$ corresponds to a FF calculated by using a template model α for a binary with masses (m_1, m_2) .

More simply, if we divide the parameter region into four subregion and employ the models in the subregions individually, an effective template family can be easily obtained. The rule to divide the parameter region is motivated by the valid criteria of the models described in the previous section. In figure 3, the left panel shows the FFs calculated by changing a total mass with a fixed mass ratio $q = 1$, and the right panel

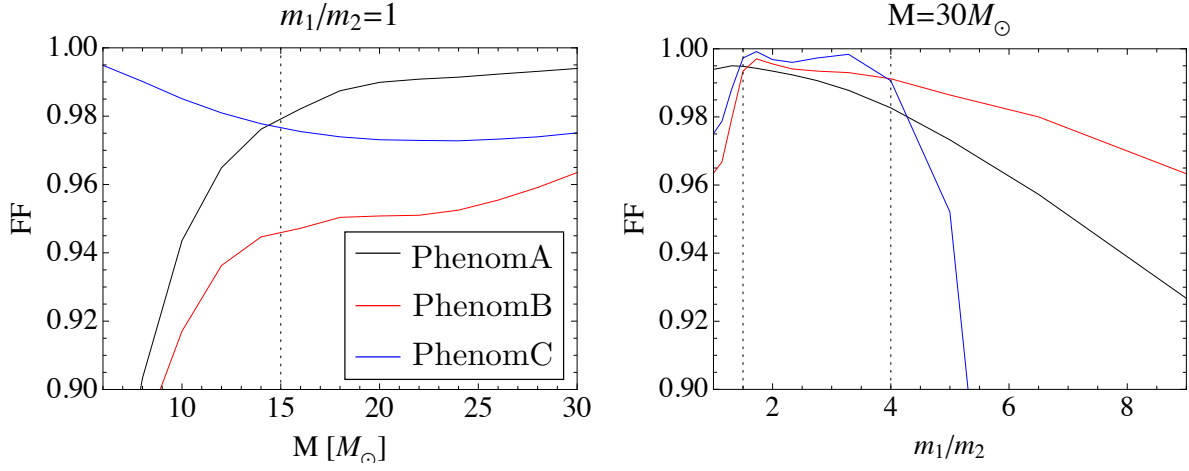


Figure 3. Fitting factors calculated by changing a total mass with a fixed mass ratio $m_1/m_2 = 1$ (left) and calculated by changing a mass ratio with a fixed total mass $M = 30M_\odot$ (right). The dotted lines indicate $M = 15M_\odot$ (left) and $q = 1.5, 4$ (right).

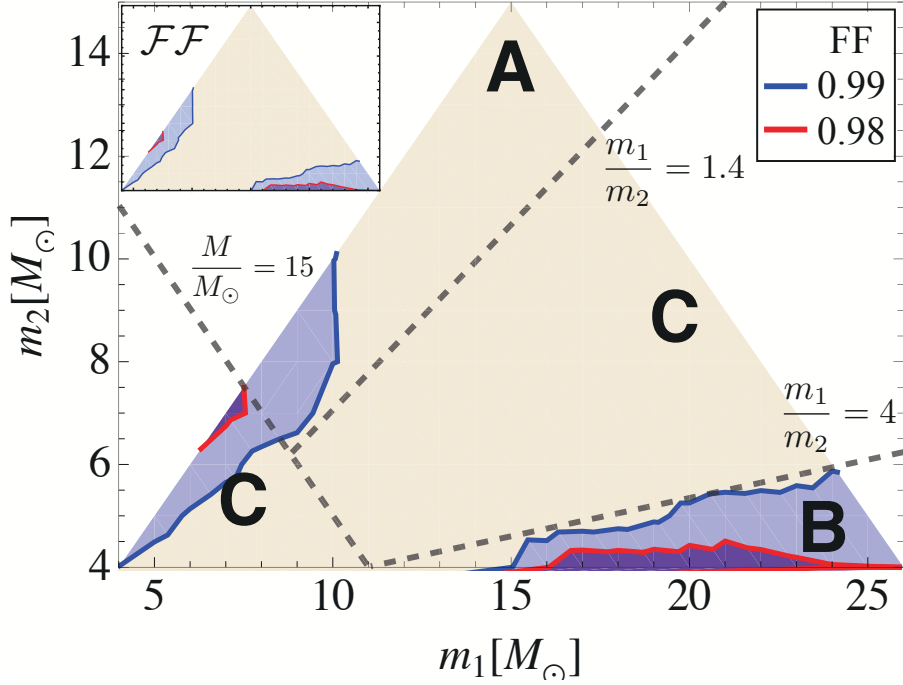


Figure 4. Fitting factors for nonspinning BBHs calculated by using the PhenomA (A), the PhenomB (B) and the PhenomC (C) individually in the four subregions divided by the dashed lines. For comparison, the FFs of the optimal template family calculated at the same parameter region is presented in the inset.

shows the FFs calculated by changing a mass ratio with a fixed total mass $M = 30M_\odot$. In the left panel, only the PhenomC is valid at the masses lower than $\sim 15M_\odot$, while the PhenomA is most efficient at $M \geq 15M_\odot$. In the right panel, the PhenomA is most efficient at $q \leq 1.5$ and the PhenomC is most efficient at $q \geq 4$. In the region

$1.5 < q < 4$, all models have the FFs greater than 0.98, but the most efficient one is the PhenomB. Note that $q = 4$ is consistent with the boundary of the valid criteria of the PhenomA and the PhenomC as described in table 1. From these features, we divide the parameter region into four subregions and construct an effective phenomenological template family as in figure 4. The effective template family is composed of PhenomC waveforms in the region $M < 15M_{\odot}$, while in the region $M \geq 15M_{\odot}$, that adopts individual models in three subregions divided by the mass ratios $q = 1.4$ (we found that choosing 1.4 instead of 1.5 can give a better result) and 4. We find that the FF contours agree well with those of the optimal template family presented in the inset. All FFs of the effective template family are better than 0.97 and mostly greater than 0.99.

4. Summary and future work

Next-generation ground-based GW detectors, such as Advanced LIGO [1] and advanced Virgo [2], will start observations in coming years. Although astrophysical BHs are likely to have spins, nonspinning binaries may be the first search targets because nonspinning searches are computationally much more cheap than spinning searches. In addition, the Fourier-domain template models should also be used for fast matched filtering. In this context, we investigated the validity of the existing phenomenological models for nonspinning BBH searches at low masses with Advanced LIGO sensitivity. Although the PhenomB and the PhenomC have been developed for spinning systems, we also applied these models to nonspinning searches by choosing zero spins. We found that the PhenomA is valid for low mass BBH searches in the region $M \geq 12M_{\odot}$ and $q \leq 4$, and the PhenomB is also valid in the region $M \geq 15M_{\odot}$ but invalid in broad asymmetric mass region. The PhenomC is most efficient among the three models, with which the FFs are always better than 0.97 in our mass region except highly asymmetric region. Especially, we proposed an effective phenomenological template family that could be easily constructed by employing the phenomenological models in the four subregions individually. The effective template family gives the FFs better than 0.97 in our entire mass region and mostly greater than 0.99. The effective template family can directly applied to the search analysis, thus that will allow us to conduct very efficient analysis for the low-mass nonspinning BBH searches with forthcoming ground-based detectors.

The necessity of using full IMR waveforms is more pronounced in high mass region because a portion of merger-ringdown phase can significantly impact the total SNR (e.g., see figure 9 in [24]). The phenomenological models are generally more efficient for high mass BBH searches. This will be studied in detail in a future work. For spinning BBHs, the PhenomB and the PhenomC have been tested for search [10, 11] and parameter estimation [25] by using nonprecessing hybrid waveforms with several spin values. The FFs of these models can also be studied in detail by exploring a three-dimensional parameter space including the spin parameter when an exact spinning EOBNR model is available.

Acknowledgments

This work used the computing resources at the KISTI Global Science Experimental Data Hub Center (GSDC).

References

- [1] Aasi J *et al* (LIGO Scientific Collaboration) 2015 *Class. Quantum Grav.* **32**, 074001
- [2] Acernese F *et al* 2015 *Class. Quantum Grav.* **32**, 024001
- [3] Abadie J *et al* (LIGO Collaboration, Virgo Collaboration) 2012 *Phys. Rev. D* **85**, 082002
- [4] Buonanno A, Iyer B R, Ochsner E, Pan Y and Sathyaprakash B S 2009 *Phys. Rev. D* **80**, 084043
- [5] Brown D A, Kumar P and Nitz A H 2013 *Phys. Rev. D* **87**, 082004
- [6] Ajith P 2008 *Class. Quantum Grav.* **25**, 114033
- [7] Cho H. -S. 2015 arXiv:1502.04399
- [8] Ajith P *et al* 2007 *Class. Quantum Grav.* **24**, S689
- [9] Ajith P *et al* 2008 *Phys. Rev. D* **77**, 104017
- [10] Ajith P *et al* 2011 *Phys. Rev. Lett.* **106**, 241101
- [11] Santamaria L *et al* 2010 *Phys. Rev. D* **82**, 064016
- [12] Hannam M *et al* 2014 *Phys. Rev. Lett.* **113**, 151101
- [13] Pan Y *et al* 2014 *Phys. Rev. D* **89**, 061501(R)
- [14] Szilágyi B *et al* 2015 arXiv:1502.04953
- [15] Pan Y *et al* 2011 *Phys. Rev. D* **84**, 124052
- [16] <https://www.lsc-group.phys.uwm.edu/daswg/projects/lal/nightly/docs/html/>
- [17] *Advanced LIGO anticipated sensitivity curves*, <https://dcc.ligo.org/LIGO-T0900288/public>
- [18] Allen B, Anderson W G, Brady P R, Brown D A and Creighton J D E 2012 *Phys. Rev. D* **85**, 122006
- [19] Apostolatos T A 1995 *Phys. Rev. D* **52**, 605
- [20] Sathyaprakash B S and Dhurandhar S V 1991 *Phys. Rev. D* **44**, 3819 .
- [21] Balasubramanian R, Sathyaprakash B S and Dhurandhar S V 1996 *Phys. Rev. D* **53**, 3033
- [22] Owen B J 1996 *Phys. Rev. D* **53**, 6749
- [23] Aasi J *et al* (LIGO Scientific Collaboration, Virgo Collaboration) 2013 *Phys. Rev. D* **87**, 022002
- [24] Ajith P and S. Bose S 2009 *Phys. Rev. D* **79**, 084032
- [25] Pürrer M, Hannam M, Ajith P and Husa S *Phys. Rev. D* **88**, 064007